

Transmission line models to simulate the impedance of the uterine vasculature during the ovarian cycle and pregnancy

Yanmei Zhu^a, Benjamin J. Sprague^{a,b}, Terrance M. Phernetton^b, Ronald R. Magness^{b,c,d}, Naomi C. Chesler^{a,*}

^a Department of Biomedical Engineering, University of Wisconsin, Madison, WI, USA

^b Department of Ob/Gyn Perinatal Research Laboratories, University of Wisconsin, Madison, WI, USA

^c Department of Animal Sciences, University of Wisconsin, Madison, WI, USA

^d Department of Pediatrics, University of Wisconsin, Madison, WI, USA

ARTICLE INFO

Keywords:

Uterine hemodynamics
Computer simulation
Resistance
Compliance

ABSTRACT

Objectives: Changes in uterine vascular impedance may yield diagnostic insight into physiological and pathological changes in uterine vascular resistance and compliance during the ovarian cycle and pregnancy. Herein, our objectives were to develop models to simulate uterine vascular impedance in order to gain insight into the vascular size and stiffness changes that occur during ovarian cycling and pregnancy.

Study design: Two electrical analogue transmission line models were developed and evaluated based on goodness-of-fit to experimental impedance measurements, which were obtained in nonpregnant luteal and follicular phase (NP-L and NP-F) and pregnant (P) ewes ($n = 4-8$ per group). First, an anatomically based, multi-segment, symmetric, branching transmission line model was developed. Parameter values were calculated based on experimental measurements of size and stiffness in the first three generations of the uterine arterial tree for NP-L, NP-F and P ewes. Then, a single segment transmission line model was developed and effective parameter values were optimized to best-fit the measured impedances.

Results: The anatomically based multi-segment model did not yield the expected good agreement with the experimental data ($R^2 < 0.5$ for all groups). In contrast, the impedance spectra predicted by the single segment model agreed very well with experimental data ($R^2 = 0.93, 0.82,$ and 0.84 for NP-L, NP-F and P, respectively; $p < 0.0001$, all groups). Furthermore, the changes in the best-fit model parameters for NP-F and P compared to the NP-L were consistent with the prior literature on the effects of the ovarian cycle and pregnancy on vascular resistance and compliance. In particular, compared to NP-L, NP-F had decreased longitudinal and terminal resistance with a modest increase in compliance whereas pregnancy caused more dramatic drops in longitudinal and terminal resistance and a significant increase in compliance.

Conclusions: The single segment transmission line model is a useful tool to examine changes in vascular structure and function that occur during the ovarian cycle and pregnancy.

© 2009 Elsevier Ireland Ltd. All rights reserved.

1. Introduction

During the ovarian cycle, changes in sex hormone (i.e., estrogen and progesterone) levels increase uterine blood flow approximately 2-fold [1–3]. Since little to no change in perfusion pressure occurs [1–3], uterine vascular resistance (UVR) decreases approximately 2-fold. In healthy pregnancies, uterine blood flow increases by 20–50-fold, again with no change in

perfusion pressure [2,4–7]; thus, UVR decreases 20–50-fold. The failure of UVR to decrease adequately with pregnancy is a hallmark of pre-eclampsia [8–11]. Increases in uterine vascular compliance also occur during pregnancy [12,13]. A decrease in systemic arterial compliance has been shown to occur with pre-eclampsia, which contributes to insufficient uterine perfusion [14,15], but the consequences of pre-eclampsia for uterine artery compliance changes during pregnancy are not known. Furthermore, the ways in which these resistance and compliance changes affect blood flow waveforms, which are measured clinically for diagnosis of pre-eclampsia with or without intrauterine growth retardation [14,16,17], are not well understood.

Uterine vascular impedance is a function of blood pressure and flow that, unlike UVR, is sensitive to changes in waveform

* Corresponding author at: Department of Biomedical Engineering, University of Wisconsin at Madison, 2146 Engineering Centers Building, 1550 Engineering Drive, Madison, WI 53706-1609, USA. Tel.: +1 608 265 8920; fax: +1 608 265 9239.

E-mail address: chesler@engr.wisc.edu (N.C. Chesler).

that are caused by longitudinal arterial resistance and arterial compliance. Whereas UVR measures the opposition to steady flow, impedance measures the opposition to pulsatile flow and is affected by pulse wave reflections in the vascular bed. Also unlike UVR, impedance is complex and frequency dependent. Thus, it can be difficult to gain simple insights into vascular structure and function changes from an experimentally measured impedance spectrum. A computer model of pulsatile blood flow dynamics in a vascular network that captures the dependencies of hemodynamic function (i.e., impedance, based on pulsatile pressure–flow relationships) on vascular structure (i.e., size, number and mechanical properties) can be a useful tool to explore mechanisms by which physiological and pathological changes in blood flow patterns arise during the ovarian cycle and with pregnancy.

Many features of pulsatile pressure and flow in a vascular system can be modeled by an electrical circuit model in which blood flow and pressure are represented by electrical current and voltage, respectively [18–20]. Either lumped parameter or transmission line models can be used, but only transmission line models capture details of wave reflections that are critical to pulsatile pressure–flow relationships [21]. Three-dimensional finite element (or finite volume or finite difference) numerical models can also be used to predict blood pressure and flow patterns but only if the walls are modeled as compliant and physiologically realistic outlet boundary conditions are used. The use of compliant walls in a complex, branching vascular network requires significant computational resources; furthermore realistic pressure and flow data below the arteriolar level in the uterine circulation are not available. Thus, here we used transmission line models to predict uterine vascular pulsatile pressure–flow relationships during the ovarian cycle and with pregnancy.

A transmission line model of the uterine vasculature was first proposed by Mo et al. [22]. This model represented each arterial segment as a resistor (R) in series with an inductor (L) to model the vessel longitudinal impedance, and one capacitor (C) to model the elasticity of the vessel wall. A terminal load resistor (R_L) ensured appropriate steady state behavior. Hill et al. [23] modified Mo's model into a viscoelastic two-load model that better fit the umbilicoplacental impedance spectra of fetal sheep.

In this study, two transmission line models were developed and evaluated for their ability to predict ovine uterine vascular impedance measured at two time points in the ovarian cycle and in pregnancy. The first was an anatomically based, multi-segment, symmetric branching model in which parameter values were selected based on experimental measurements. The second was a single-segment, effective model in which parameters values were optimized to best-fit experimentally obtained impedance spectra. The effects of the ovarian cycle and pregnancy on parameter values were investigated. In addition, we investigated the effects of the single-segment model parameter values on impedance spectra and blood flow.

2. Materials and methods

2.1. Transmission line models

Based on the work by Mo et al. [22], we modeled a single artery in the uterine arterial tree with a distributed resistor (R) in series with a distributed inductor (L) representing the vessel longitudinal resistance and inductance, respectively, and one distributed capacitor (C) representing the elasticity of the vessel wall. For any given arterial segment in the transmission line model, the propagation coefficient (γ) and characteristic impedance (Z_C) for

each segment are calculated as

$$\gamma = \sqrt{(R + j\omega L)(j\omega C)} \quad (1)$$

$$Z_C = \sqrt{\frac{R + j\omega L}{j\omega C}} \quad (2)$$

where $j = \sqrt{-1}$ and ω is the radial frequency ($\omega = 2\pi f$ where f is a frequency component of the heart rate) [24]. For a segment of length l , if the downstream load impedance is Z_L , the input impedance upstream is [24]

$$Z_{in} = Z_C \frac{[Z_L + Z_C \tanh(\gamma l)]}{[Z_C + Z_L \tanh(\gamma l)]} \quad (3)$$

A preliminary analysis of uterine arterial tree structures in pregnant and nonpregnant ewes (see Fig. 1) revealed no significant differences in number of arteries in the first three generations. Therefore, for our anatomically based transmission line model, we used the same basic structure for nonpregnant and pregnant cases. In particular, a three-level symmetric branching tree structure in which four identical daughter branches (tertiary, $k = 3$) originated from each of two identical daughter branches (secondary, $k = 2$), which originated from the main uterine artery (primary, $k = 1$), was assumed (Fig. 2A). Then, for all identical segments at a given level k :

$$Z_{k,in} = Z_{k,C} \frac{[Z_{k,L} + Z_{k,C} \tanh(\gamma_k l_k)]}{[Z_{k,C} + Z_{k,L} \tanh(\gamma_k l_k)]} \quad (4)$$

And because of the symmetry of the branching structure

$$Z_{k,L} = \frac{1}{n_{k+1}} Z_{(k+1),in} \quad (5)$$

where n_{k+1} is the number of identical elements that originate from the end of segment k and which constitute the segments at level $k + 1$. For the tertiary branches ($k = 3$), $n_{k+1} = 1$ and the terminal load impedance was assumed to be a pure resistance such that $Z_{3,L} = R_L$ (Fig. 2A).

Parameter values for this multi-segment, symmetric branching model were based on experimental measurements of primary, secondary and tertiary arteries in the uterine vascular bed in nonpregnant (both follicular and luteal phase) and pregnant ewes. To calculate these parameter values, we made several assumptions

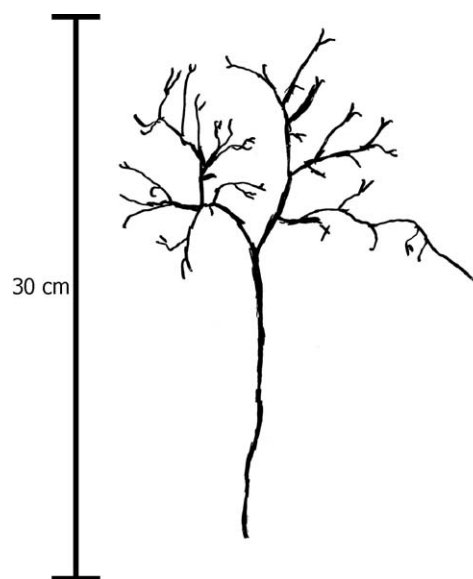


Fig. 1. A representative Mercox casting of the uterine arterial tree from a single horn of a nonpregnant ewe.

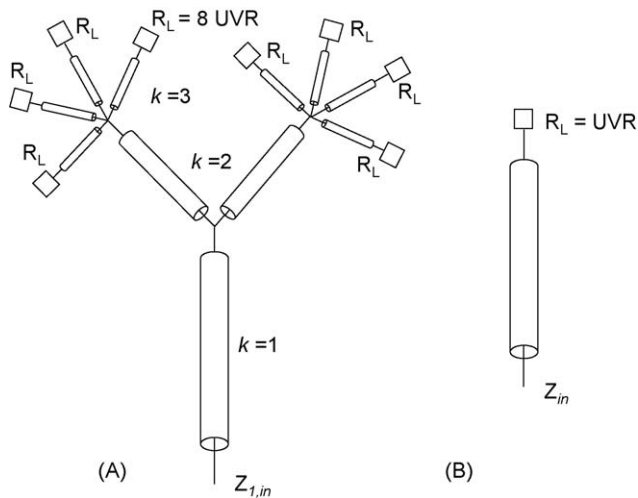


Fig. 2. Transmission line models used to simulate the ovine uterine vasculature impedance. (A) Anatomically based, multi-segment, symmetric branching model and (B) single-segment effective model.

consistent with the prior literature [18,19,22]. First, blood was assumed to be Newtonian and incompressible such that the Navier–Stokes equations could be used. Second, blood flow in each arterial segment was assumed to be fully developed and symmetric about the axis. Third, leakage from the small branches of the main artery that supply the cervix area were ignored. And, fourth, we assumed that artery walls were linearly elastic and nonviscous with elastic modulus E_k . Given these assumptions, the parameter values R_k , L_k and C_k were [25]

$$R_k = \frac{8\mu}{\pi r_k^4} l_k \left[\frac{Ns}{m^5} \right] \quad (6)$$

$$L_k = \frac{9\rho}{4\pi r_k^2} l_k \left[\frac{Ns^2}{m^5} \right] \quad (7)$$

$$C_k = \frac{3\pi r_k^3}{2E_k h_k} l_k \left[\frac{m^5}{N} \right] \quad (8)$$

where r_k is the vessel internal radius at a physiological pressure, E_k is the Young's modulus of the vessel wall, h_k is vessel wall thickness, and l_k is the segment length, for each identical segment in a single generation of the arterial tree ($k = 1, 2$ or 3), and ρ is the mass density of blood, and μ is the blood viscosity. Blood density and viscosity values of 1060 kg/m^3 and $3.9 \times 10^{-3} \text{ Pa s}$, respectively, were used. The methods used to experimentally measure r_k , E_k , and h_k , as well as l_k , are described below (Section 2.2). The terminal load resistance (R_L) was set equal to the primary artery input impedance $Z_{1,in}$ at 0 Hz (equal to UVR) times the number of (identical) terminal load resistors since they all act in parallel. For the branching structure assumed here, $R_L = 8 \text{ UVR}$.

We also developed a non-anatomical single-segment transmission line that “effectively” represents the uterine vasculature (Fig. 2B). Hence, we call it a single-segment effective transmission line model. In this case, the parameters R , L , C and transmission line length l do not reflect characteristics of individual arterial segments but the overall arterial network behavior. For a single-segment transmission line, $Z_{1,in}$ is given by Eq. (4) with $R_L = \text{UVR}$. For this model, the method of least squares was used to find the model parameter values R , L , C and l that best fit the experimentally obtained uterine vascular impedance spectra. The Nelder–Mead simplex (direct search) method was used to minimize the sum of squared differences between the measured and predicted values with the constraint that the parameter values had to be positive.

Both the multi-segment and single-segment effective models were implemented in MATLAB (The MathWorks Inc., Natick, MA). Predicted input impedance spectra were calculated based on the appropriate set of parameter values in the frequency range of interest (0–10 Hz). The maximum frequency (10 Hz) was chosen to be five times the normal heart rate ($\sim 2 \text{ Hz}$). The models were first used to repeat Hill's work [23] on wave transmission model in the umbilicoplacental circulation. Once the computations were thus checked, each model was used to calculate the uterine vascular impedance magnitude spectra in the nonpregnant luteal phase (NP-L), nonpregnant follicular phase (NP-F) or pregnant (P) state. Goodness-of-fit was evaluated based on the square of the correlation coefficient between the predicted and measured impedance spectra (R^2 value) and the significance of the correlation (p value).

2.2. Experimental data collection

Procedures for animal handling and protocols for experiments were approved by the University of Wisconsin–Madison Research and Animal Care and Use Committees of both the Medical School and the College of Agriculture and Life Sciences. Data from three groups of multiparous female sheep of mixed western breeds were used: two nonpregnant groups in different phases of the ovarian cycle and one late-gestation, pregnant group. The nonpregnant (NP) animals ($n = 13$) were experimentally synchronized and sacrificed during two distinct controlled points of the ovarian cycle. These were the late follicular phase during the peri-ovulatory period (NP-F, $n = 7$) and the late luteal phase 10–11 days post-ovulation (NP-L, $n = 6$) as described previously [26]. The pregnant group (P, $n = 10$) were studied at 120–130 days gestation. The natural gestation length for sheep is 145–147 days.

Uterine arterial blood pressure (UAP) and heart rate (HR) were measured via a fluid-filled catheter inserted near the uterine artery, after anesthetization. Uterine blood flow (UBF) through the primary uterine artery was measured using a 3 mm or 6 mm ultrasound probe (3RS and 6RS probes, Transonic Systems Inc., Ithaca, NY), depending on the size of the vessel. UAP, HR and UBF were sampled simultaneously at 1000 Hz using WinDaq Pro Data Acquisition software (DATAQ Instruments, Akron, OH).

To calculate experimental uterine vascular impedance spectra, UAP and UBF waveforms for ten sequential cardiac cycles were isolated and independently analyzed. Values were averaged for each animal. Coefficients of variation within each animal were less than 8%. Digital signal processing prior to frequency analysis included Hann windowing and zero-padding. These processed waveforms were then resolved into their frequency components using a discrete fast Fourier transform. The ratio of pressure to flow at each harmonic of the heart rate was computed as previously described [11,17,27]. Here we consider only impedance magnitude because the distance between the sites of pressure and flow measurement made the impedance phase calculation unreliable and because the impedance magnitude typically contains more clinically relevant information [28].

After the hemodynamic measurements were obtained, right and left uterine artery outer diameters were measured ($OD_{in vivo}$). Following sacrifice and hysterectomy, the uterine artery branching networks from each horn of the uterus were dissected and kept intact. Within 30 min, Mercor acrylic casting material was perfused into the artery network until the left and right uterine artery outer diameters matched the $OD_{in vivo}$ measurements. Then, outer diameters throughout the Mercor-filled arterial network were measured (OD_m). Within 10 min the Mercor solidified, producing an internal cast of the pressurized arterial network. The

first three generations of the uterine vascular tree were then traced and labeled in this inflated state (Fig. 1); measurements of artery inner diameter (ID_m) and length ($Length_m$) were made from the casting material. At least two measurements were made at each level in each animal. Finally, from the ID_m , $Length_m$ and OD_m measurements, wall thickness (WT_m) was calculated for each generation in the arterial tree assuming conservation of mass. Single values for $ID_{m,k}$, $WT_{m,k}$ and $Length_{m,k}$ for each $k = 1, 2$ and 3 were obtained for each animal based on an average of 2–4 arteries. These values were then averaged for each group (NP-L, NP-F and P) and standard error was calculated.

Second generation arteries from each uterine arterial network were harvested for measurement of circumferential elastic modulus E as described in detail elsewhere in this issue [29]. Briefly, arteries were isolated, harvested and perfused *ex vivo*. Outer diameter and length were measured during pressurization from 0 to 120 mmHg in 10 mmHg increments. Circumferential stress and strain were calculated using standard formulations and the slope in a physiological pressure range was taken as E . For additional methodological details, we refer the reader to [29].

3. Results

3.1. Measured impedance

The measured impedance magnitude spectra for the luteal and follicular phase and pregnant ewes are shown in Fig. 3. As expected, pregnancy decreased the impedance dramatically compared to the two nonpregnant cases for all frequencies. Impedance magnitude in the follicular phase was also lower than in the luteal phase at all frequencies. In both nonpregnant cases, the impedance reached a minimum at the 6th harmonic and a maximum between the 8th and 9th harmonics. In the pregnant case, the impedance reached a minimum near the 5th harmonic and a maximum at the 8th harmonic, at which point it was nearly equal to the input resistance (at 0 Hz) in magnitude.

3.2. Anatomically based, multi-segment model

Experimental measurements of ID_m , WT_m and $Length_m$ for each of the first three generations of the uterine arterial network ($k = 1, 2, 3$), and E for second-generation arteries, for luteal and follicular phase and pregnant ewes are shown in Table 1. R_k , L_k , and C_k were calculated from these data according to Eqs. (6)–(8), assuming $E_1 = E_2 = E_3$ for all groups (Table 2). I_k was set equal to $Length_m$ for each k , and R_L was set equal to 8 UVR as described above.

The predicted input impedance magnitude spectrum at the primary uterine artery ($Z_{1,in}$) was computed using Eqs. (4) and (5) in an iterative fashion. As shown in Fig. 4, the agreement with the experimentally obtained impedance spectra was poor. All correlation coefficients (R^2 values) were less than 0.5. All predicted spectra matched measured spectra at 0 Hz because $Z_{1,in}$ was constrained to UVR at 0 Hz.

Since elastic modulus is known to increase with increasing distance from the heart [30], we also tested the effects of letting $1/2E_1 = E_2 = 2E_3$ as an upper bound on this effect (data not shown). In the nonpregnant cases, this caused the second peaks to shift from the 9th and 10th harmonics (for the NP-F and NP-L, respectively) to the 8th and 9th harmonics. In the pregnant case, this caused three small peaks to occur at the 3rd, 6th and 9th harmonics instead of the medium-sized peaks between the 3rd and 4th, and 7th and 8th harmonics as in Fig. 4B. In no case did this change improve the goodness-of-fit of the predicted impedance to the measured impedance ($R^2 < 0.5$; $p > 0.05$ for NP-L, NP-F and P).

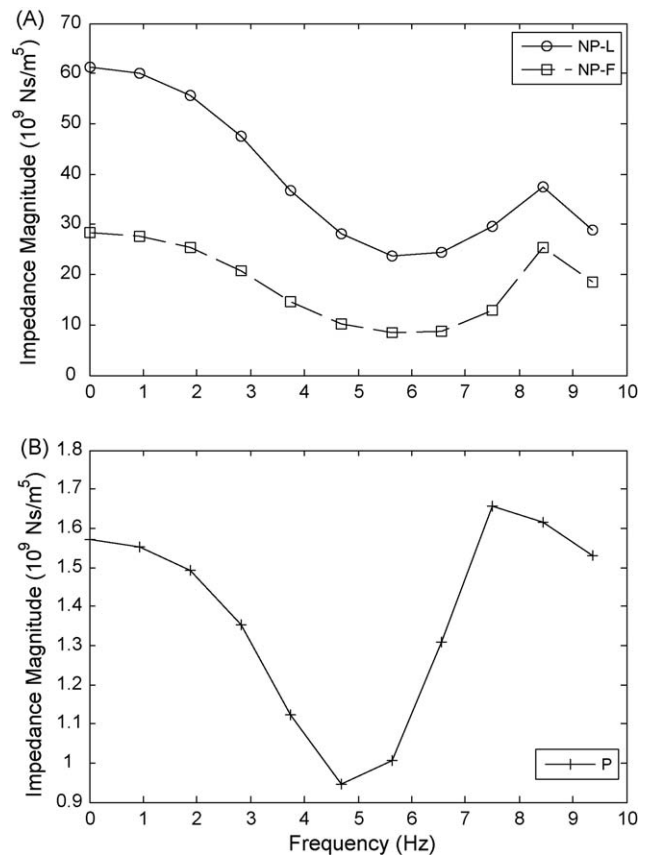


Fig. 3. Experimental uterine vascular impedance magnitude spectra for (A) luteal and follicular phase and (B) pregnant ewes.

3.3. Single-segment model

The best-fit R , L , C and I values for the single-segment transmission line model of uterine vascular impedance for the luteal and follicular phase and pregnant ewes are given in Table 3. In contrast to the anatomically based multi-segment model, the single-segment model yielded impedance spectra that agreed well with experimental data ($R^2 = 0.94, 0.84$ and 0.87 for luteal, follicular and pregnant, respectively; Fig. 5). All correlations were also highly significant ($p < 0.0001$ for all groups).

Compared to the luteal phase, best-fit length was relatively unchanged in the follicular phase but inertance L was nearly half, compliance C was approximately double and longitudinal resistance was five orders of magnitude less ($\sim 1 \times 10^5$ Ns/m⁶). With pregnancy, length approximately tripled, L decreased 30-fold, C

Table 1

Experimental measurements of uterine artery inner diameter (ID_m), wall thickness (WT_m) and length ($Length_m$) in each of the first three generations of the uterine arterial network ($k = 1, 2, 3$) for luteal and follicular phase and pregnant ewes.

| State | k | ID_m (mm) | WT_m (mm) | $Length_m$ (cm) | E (kPa) |
|------------|-----|-------------|-------------|-----------------|-----------|
| Luteal | 1 | 2.80 ± 0.40 | 0.42 ± 0.05 | 14.60 ± 1.30 | 265 ± 19 |
| | 2 | 2.20 ± 0.25 | 0.32 ± 0.03 | 4.51 ± 1.01 | |
| | 3 | 1.63 ± 0.09 | 0.30 ± 0.02 | 2.80 ± 0.64 | |
| Follicular | 1 | 3.30 ± 0.21 | 0.38 ± 0.07 | 15.41 ± 1.33 | 250 ± 21 |
| | 2 | 2.30 ± 0.18 | 0.36 ± 0.03 | 4.74 ± 0.74 | |
| | 3 | 1.68 ± 0.16 | 0.31 ± 0.02 | 2.79 ± 0.48 | |
| Pregnant | 1 | 5.92 ± 0.16 | 0.31 ± 0.02 | 24.24 ± 1.24 | 168 ± 18 |
| | 2 | 4.59 ± 0.25 | 0.29 ± 0.02 | 3.87 ± 0.67 | |
| | 3 | 2.61 ± 0.19 | 0.30 ± 0.04 | 3.54 ± 0.54 | |

Circumferential elastic modulus (E) was measured in secondary generation arteries only. Mean values ± standard error shown for all measurements.

Table 2

Parameters values for the multi-segment transmission line model in which, for each generation of the uterine arterial tree ($k = 1, 2, 3$), longitudinal resistance and inductance, and transverse compliance (R, L , and C , respectively) per unit length (l), were modeled with distributed elements based on experimental measurements.

| State | k | R/l ($\times 10^9 \text{Ns/m}^6$) | L/l ($\times 10^9 \text{Ns}^2/\text{m}^6$) | C/l ($\times 10^{-9} \text{m}^4/\text{N}$) | R_L ($\times 10^9 \text{Ns/m}^5$) |
|------------|-----|--|---|---|--|
| Luteal | 1 | 2.58 | 0.39 | 0.12 | 490 |
| | 2 | 6.78 | 0.63 | 0.07 | |
| | 3 | 22.5 | 1.14 | 0.03 | |
| Follicular | 1 | 1.34 | 0.28 | 0.22 | 227 |
| | 2 | 5.68 | 0.57 | 0.08 | |
| | 3 | 19.95 | 1.08 | 0.04 | |
| Pregnant | 1 | 0.13 | 0.09 | 2.35 | 12.5 |
| | 2 | 0.36 | 0.14 | 1.17 | |
| | 3 | 3.42 | 0.45 | 0.21 | |

Terminal downstream resistance (R_L) was calculated based on the primary artery input impedance at 0 Hz equal to the UVR. For the idealized branching structure assumed here, $R_L = 8 \text{ UVR}$.

increased 6-fold, and R remained small ($\sim 1 \times 10^5 \text{Ns/m}^6$). R_L changed according to the measured changes in UVR by constraint.

3.4. Impedance shape and blood flow magnitude sensitivity analysis

To demonstrate the dependence of the shape of the impedance spectra on parameter values, we changed parameter values by plus or minus 20% of the original value (one at a time) and calculated the impedance spectra. Due to the large number of degrees of

Table 3

Parameters values for the single-segment effective transmission line model in which longitudinal resistance and inductance, and transverse compliance (R, L , and C , respectively) per unit length (l), were modeled with distributed elements based on best-fit to the experimental measurements of uterine vascular impedance for luteal and follicular phase and pregnant ewes.

| | l (m) | R/l ($\times 10^9 \text{Ns/m}^6$) | L/l ($\times 10^9 \text{Ns}^2/\text{m}^6$) | C/l ($\times 10^{-9} \text{m}^4/\text{N}$) | R_L ($\times 10^9 \text{Ns/m}^5$) |
|------------|---------|--|---|---|--|
| Luteal | 0.10 | 24.8 | 14.8 | 0.01 | 61 |
| Follicular | 0.11 | ~ 0 | 7.3 | 0.02 | 28 |
| Pregnant | 0.33 | ~ 0 | 0.2 | 0.13 | 1.6 |

Best-fit was optimized over positive values of l, R, L and C with $R_L = \text{UVR}$ by constraint.

freedom in the multi-segment model, we used the single-segment model and only present data for the luteal phase and pregnant spectra (Fig. 6). As expected, increasing UVR (which is equal to R_L in this case) increased the input resistance. Increasing UVR also decreased the minimum impedance value (near 7 Hz for luteal, 4 Hz for pregnant), presumably because large- and medium-sized arteries were more inflated due to the higher pressure. Decreasing UVR also decreased the variability in Z as a function of frequency (most obviously in the pregnant case; blue dashed line). Decreasing transverse arterial compliance C increased the magnitude of the minimum impedance and also shifted its location to a slightly higher frequency. It did not affect the magnitude of the input resistance or second peak magnitude (evident in the pregnant case). Finally, increasing the inductance L shifted the minimum impedance magnitude to a lower frequency and

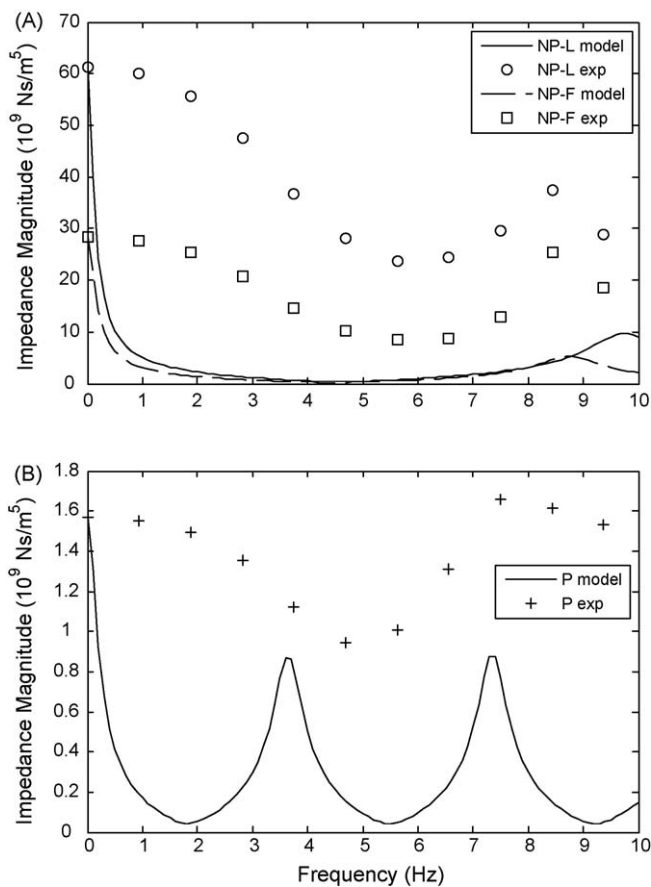


Fig. 4. Experimental measurements (symbols) and multi-segment model prediction (line) of uterine vascular impedance magnitude for (A) luteal and follicular phase ($R^2 = 0.30$ and 0.27 , respectively; $p > 0.05$) (B) and pregnant ewes ($R^2 = 0.04$; $p > 0.05$). See Table 2 for parameter values.

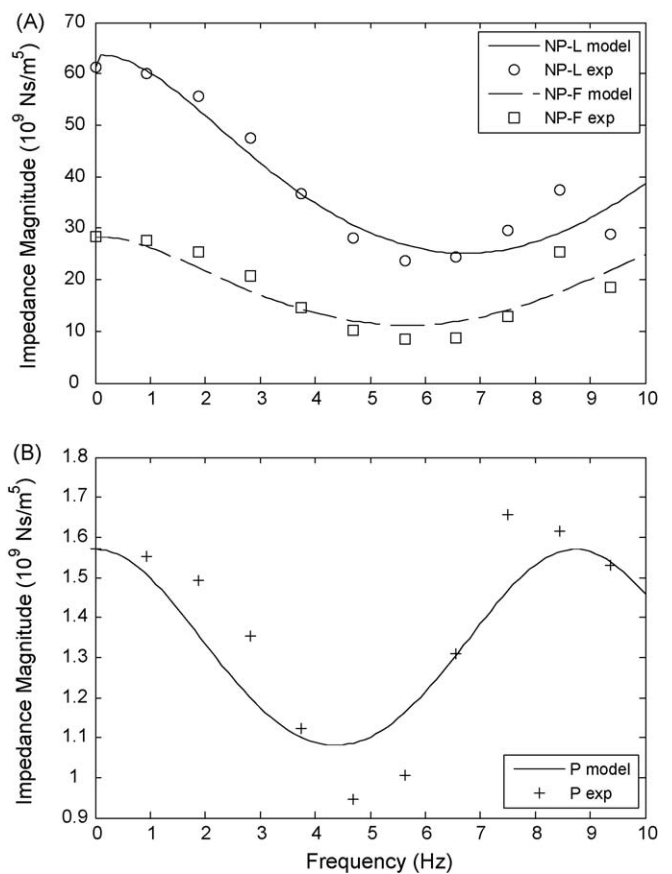


Fig. 5. Experimental measurements (symbols) and single-segment effective model prediction (line) of uterine vascular impedance magnitude for (A) luteal and follicular phase ($R^2 = 0.93$ and 0.82 , respectively; $p < 0.0001$) and (B) pregnant ewes ($R^2 = 0.84$; $p < 0.0001$). See Table 3 for parameter values.

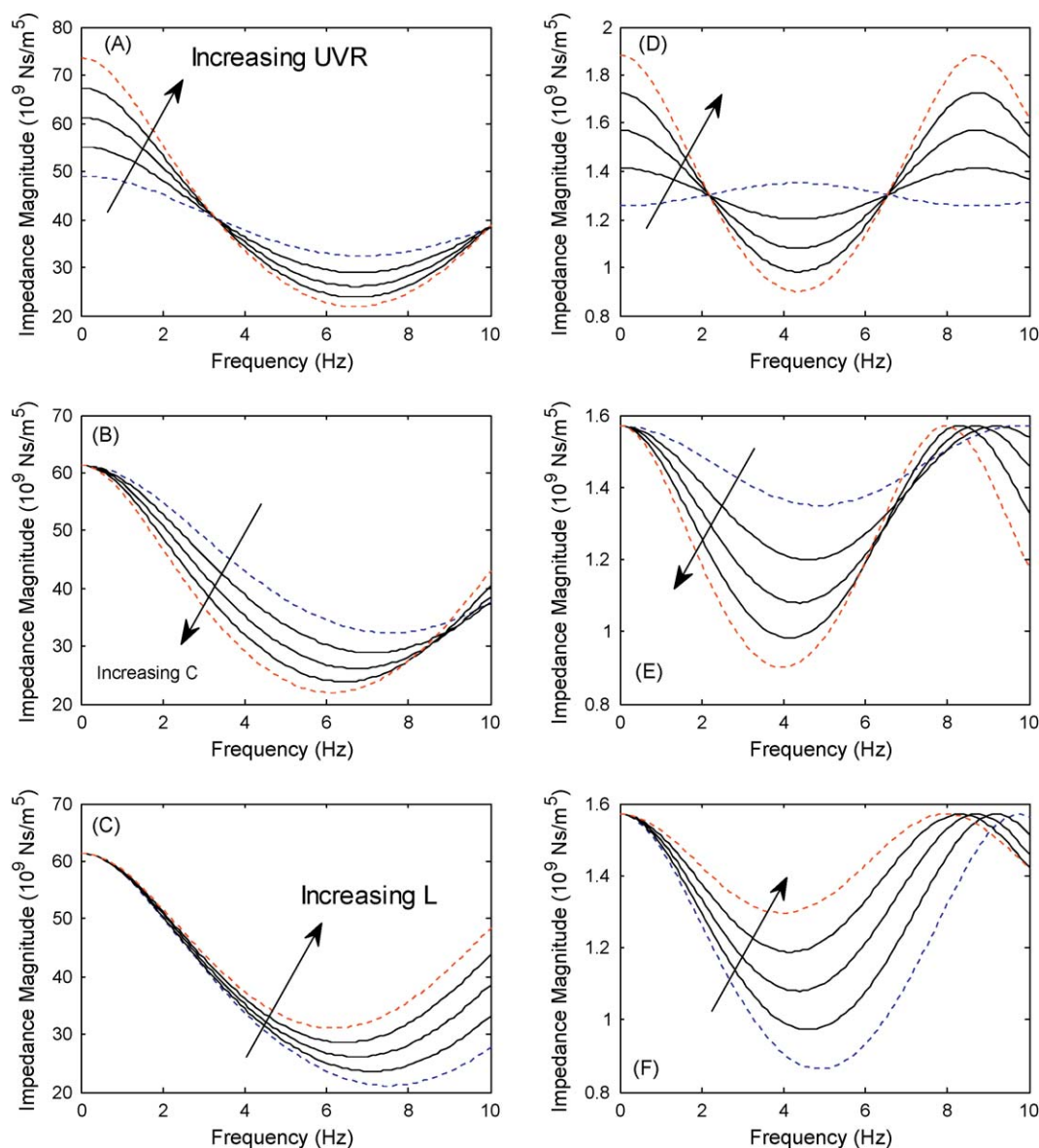


Fig. 6. Predicted impedance spectra for (A–C) luteal phase and (D–F) pregnant ewes for variations in (A, D) UVR , (B, E) C and (D, F) L in the single-segment effective transmission line model. In each case, parameter values were varied by $\pm 20\%$ of measured (UVR) or best-fit (Table 3) parameter values. Effects of increasing parameter values are shown with upward pointing arrows. Blue is 80% value; Red is 120% value.

increased its amplitude. Like C , it did not affect the magnitude of the input resistance or second peak magnitude. In general we found that the magnitude of the first minimum was determined by $L/(UVR C)$ and the frequencies of the first minimum and second peak were determined by $1/LC$.

As a consequence of these changes in spectra, for any pressure waveform, the flow waveform into the uterine vasculature will change. To demonstrate, we imposed a sinusoidal pressure waveform at 2 Hz ($HR = 120$ bpm) with mean pressure of 100 mmHg and a pulse pressure of 40 mmHg. The resulting predicted mean UBF for the range of UVR , C and L values used above (Fig. 6) are shown in Fig. 7. As expected, the mean UBF is strongly inversely dependent on UVR . Since decreasing C tends to increase impedance near 2 Hz, the consequence of decreasing C is to decrease blood flow for the same driving pressure. Changing L by $\pm 20\%$ of the best-fit value has little effect on the impedance magnitude near 2 Hz, so varying L in this range has minimal effect on mean blood flow. Overall, the effects of these parameters in the luteal and follicular (not shown) phase and in pregnancy are similar.

4. Discussion

Here we present two transmission line models of the uterine vasculature in order to gain insight into the vascular size and stiffness changes that occur during the ovarian cycle and with pregnancy. Our major findings are that the effects of the ovarian cycle and pregnancy on the vasculature can be represented by decreased longitudinal and terminal resistance with a modest increase in compliance in the follicular phase (compared to the luteal phase) and more dramatic drops in longitudinal and terminal resistance and a significant increase in compliance with pregnancy.

We note that the anatomically based, multi-segment, symmetric branching transmission line model poorly predicted the measured impedance spectra for all groups (NP-L, NP-F and P). The values used to calculate the model parameters, including r_k , h_k , and l_k , were measured directly from luteal and follicular phase and pregnant ewes in multiple branches in three generations of the arterial tree. However, we made several assumptions that likely

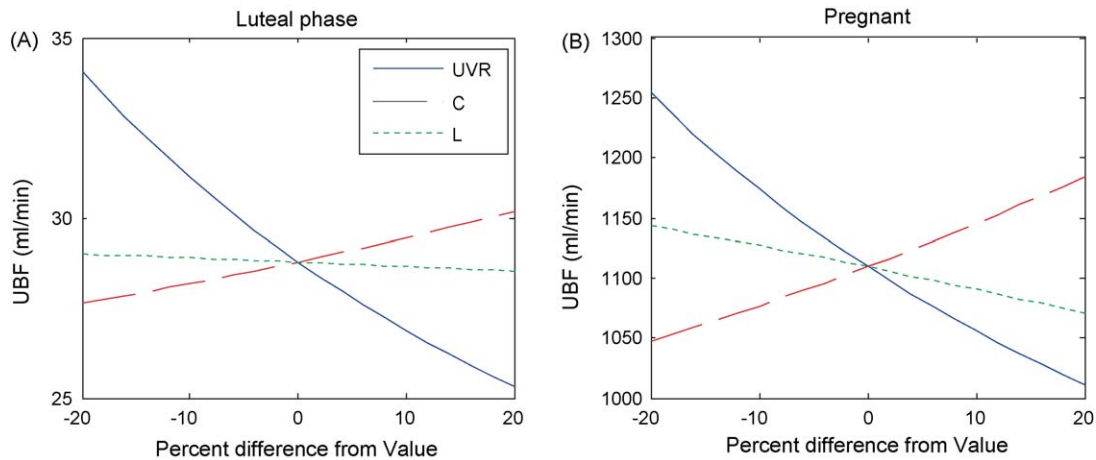


Fig. 7. Predicted effects of variations in UVR, C and L on mean UBF for (A) luteal phase and (B) pregnant ewes. In each case, parameter values were varied by $\pm 20\%$ of measured (UVR) or best-fit parameter values (Table 3). Effects of increasing UVR are in blue, solid; effects of increasing C are in red, dashed; effects of increasing L are in green, dotted. Note difference in scale from (A) to (B).

decreased the accuracy of the multi-segment model predictions. First, we assumed a symmetric branching structure. As is evident from Fig. 1, this assumption is not valid. However, creating "patient-specific" geometries in order to mimic an individual impedance spectrum was not the goal of this work. Here, we sought to understand the uterine vascular hemodynamic changes during the ovarian cycle and with pregnancy, which required some simplifications in anatomical structure. In future studies, we intend to test the ability of a multi-segment model to mimic the impedance in a single ewe based on detailed measurements from the uterine arterial network of that ewe. Second, we did not include arterial viscoelasticity or Womersley-type flow resistance as done by [31] in the fetal circulation, for example. Finally, we only modeled three generations of the uterine arterial network. Modeling additional levels with measured or estimated size and stiffness values may improve accuracy.

Using a single-segment effective transmission line model and the method of least squares to obtain optimized parameter values enabled excellent fitting of the experimental hemodynamic data ($R^2 > 0.8$ for all groups). We note that our optimization algorithm may have found local minima and not the global minima of the target functions. However, the changes in length predicted by the NP-L, NP-F and P optimizations agree well with our experimental data (Table 1), which suggests that the minima represent physiologically meaningful states. Furthermore, we ran the optimizations for several different sets of initial values and consistently obtained the set of best-fit parameter values reported here (Table 3).

The predicted uterine vascular changes in pregnancy – a decrease in R and increase in C – agree with our own experimental data (Table 1 and [29]) and others' data obtained in other species [12,13,32,33]. The effects of the ovarian cycle on uterine artery size or stiffness have not been as well studied. Our own experimental data have demonstrated that UVR decreases in the follicular phase compared to the luteal phase and secondary generation uterine artery elastic modulus tends to decrease as well (Table 1 and [29]). These findings are consistent with the single-segment effective model predictions that terminal load impedance decreases and compliance increases (somewhat) with the follicular phase. Our model results also suggest two other potential effects of the ovarian cycle on uterine arterial size and stiffness that warrant further investigation. First, the decrease in longitudinal resistance with minimal lengthening suggests that mid-size arteries – larger than resistance arteries and smaller than the main conduit arteries – dilate significantly in response to circulating hormone levels.

Second, the 2-fold drop in inertance suggests an increase in arterial size at one or several levels in the arterial tree.

It is worth noting here that the single-segment model is an "effective" model; that is, it simulates the impedance spectra with parameter values that are devoid of physical meaning. In particular, considering Eqs. (6) and (7), the changes in R and L predicted between the luteal and follicular phase (Table 3) cannot be explained by a change in radius in a single artery with the characteristics of the single-segment transmission line. Instead, R and L and also l and C represent bulk characteristics of the system and likely reflect changes in multiple or different segments of the actual uterine arterial tree. While these bulk characteristics are devoid of precise anatomical information, they do predict the hemodynamic behavior of the uterine arterial network during the ovarian cycle and with pregnancy, and may lead to clinically useful insights in cases of abnormal uterine arterial hemodynamics.

Finally, we investigated the impact of single model parameters on the shape of whole impedance spectra and mean blood flow. In accordance with linear transmission line theory, we found that the input resistance is determined by UVR, the magnitude of the first minimum is determined by $L/(UVR C)$, and the frequencies of the first minimum and second peak are determined by $1/LC$. In the frequency range of the normal sheep heart rate (~ 2 Hz) [34], mean UBF decreases with increasing UVR, increases with increasing C , and decreases slightly with increasing L in both the luteal phase and with pregnancy. These findings are in accordance with prior data showing that transformation of the uteroplacental bed (to decrease UVR) and remodeling of large arteries (to increase compliance and diameter) [12,13,32,33,35–37] are all important to the dramatic increase in blood flow that accompanies a healthy pregnancy.

5. Conclusion

In this study, electrical analog transmission line models were used to simulate the input impedance of the ovine uterine vascular circulation for nonpregnant and pregnant conditions. Two models, including an anatomically based, multi-segment, symmetric branching model with parameter values based on experimental measurements and a single-segment effective model with parameter values based on optimization to measured impedance spectra, were developed. The impedance characteristics of the uterine circulation were better simulated by the latter method for all conditions. The variations in the parameter values over the ovarian cycle and with pregnancy were in agreement with

available data on the effects of the ovarian cycle and pregnancy on uterine artery dimensions and mechanical properties. The single-segment model was also used to explore the dependencies of impedance spectra and mean blood flow at physiological conditions (heart rate and pressure) on uterine vascular structure and function. In future work, we plan to use this model to investigate parameters that may be useful for the diagnosis of pathologies of pregnancy such as pre-eclampsia with and without intrauterine growth retardation.

Conflict of interest statement

None declared.

Condensation

A single-segment transmission line model demonstrates that impedance changes with ovarian cycling and pregnancy are caused by changes in longitudinal and terminal resistance and compliance.

Acknowledgements

The present study was supported in part by NIH grants HL49210, HL087144, HD38843, (R.R.M.) and HL086939 (N.C.C.). The authors would also like to thank Professors Susan Hagness and Nico Westerhof for insightful comments on the modeling approaches.

References

- [1] Huckabee WE, Crenshaw C, Curet LB, Mann L, Barron DH. The effect of exogenous oestrogen on the blood flow and oxygen consumption of the uterus of the non-pregnant ewe. *Q J Exp Physiol Cogn Med Sci* 1970;55:16–24.
- [2] Magness RR, Parker Jr CR, Rosenfeld CR. Systemic and uterine responses to chronic infusion of estradiol-17 beta. *Am J Physiol* 1993;265:E690–8.
- [3] Magness RR, Phernetton TM, Gibson TC, Chen DB. Uterine blood flow responses to ICI 182 780 in ovariectomized oestradiol-17beta-treated, intact follicular and pregnant sheep. *J Physiol* 2005;565:71–83.
- [4] Zoma W, Baker RS, Lang U, Clark KE. Hemodynamic response to tibolone in reproductive and nonreproductive tissues in the sheep. *Am J Obstet Gynecol* 2001;184:544–51.
- [5] Bruce NW. The effect of ligating a uterine artery on fetal and placental development in the rat. *Biol Reprod* 1976;14:246–7.
- [6] Fuller EO, Galletti PM, Takeuchi T. Major and collateral components of blood flow to pregnant sheep uterus. *Am J Physiol* 1975;229:279–85.
- [7] Palmer SK, Zamudio S, Coffin C, Parker S, Stamm E, Moore LG. Quantitative estimation of human uterine artery blood flow and pelvic blood flow redistribution in pregnancy. *Obstet Gynecol* 1992;80:1000–6.
- [8] Naeye RL. Causes and consequences of placental growth retardation. *JAMA* 1978;239:1145–7.
- [9] Saftlas AF, Olson DR, Franks AL, Atrash HK, Pokras R. Epidemiology of pre-eclampsia and eclampsia in the United States, 1979–1986. *Am J Obstet Gynecol* 1990;163:460–5.
- [10] Papageorghiou AT, Yu CK, Nicolaides KH. The role of uterine artery Doppler in predicting adverse pregnancy outcome. *Best Pract Res Clin Obstet Gynaecol* 2004;18:383–96.
- [11] Cnossen JS, Morris RK, ter Riet G, Mol BW, van der Post JA, Coomarasamy A, et al. Use of uterine artery Doppler ultrasonography to predict pre-eclampsia and intrauterine growth restriction: a systematic review and bivariable meta-analysis. *CMAJ* 2008;178:701–11.
- [12] Mackey K, Meyer MC, Stirewalt WS, Starcher BC, McLaughlin MK. Composition and mechanics of mesenteric resistance arteries from pregnant rats. *Am J Physiol* 1992;263:R2–8.
- [13] Osol G, Cipolla M. Pregnancy-induced changes in the three-dimensional mechanical properties of pressurized rat uteroplacental (radial) arteries. *Am J Obstet Gynecol* 1993;168:268–74.
- [14] Ronnback M, Lampinen K, Groop PH, Kaaja R. Pulse wave reflection in currently and previously preeclamptic women. *Hypertens Pregnancy* 2005;24:171–80.
- [15] Tihtonen KM, Koobi T, Uotila JT. Arterial stiffness in preeclamptic and chronic hypertensive pregnancies. *Eur J Obstet Gynecol Reprod Biol* 2006;128:180–6.
- [16] McCowan LM, Ritchie K, Mo LY, Bascom PA, Sherret H. Uterine artery flow velocity waveforms in normal and growth-retarded pregnancies. *Am J Obstet Gynecol* 1988;158:499–504.
- [17] Sritippayawan S, Phupong V. Risk assessment of preeclampsia in advanced maternal age by uterine arteries Doppler at 17–21 weeks of gestation. *J Med Assoc Thai* 2007;90:1281–6.
- [18] Jager GN, Westerhof N, Noordergraaf A. Oscillatory flow impedance in electrical analog of arterial system: representation of sleeve effect and non-Newtonian properties of blood. *Circ Res* 1965;16:121–33.
- [19] Rideout VC, Dick DE. Difference-differential equations for fluid flow in distensible tubes. *IEEE Trans Biomed Eng* 1967;14:171–7.
- [20] Westerhof N, Bosman F, De Vries CJ, Noordergraaf A. Analog studies of the human systemic arterial tree. *J Biomech* 1969;2:121–43.
- [21] Westerhof N, Lankhaar JW, Westerhof BE. The arterial Windkessel. *Med Biol Eng Comput* 2008;June.
- [22] Mo LY, Bascom PA, Ritchie K, McCowan LM. A transmission line modelling approach to the interpretation of uterine Doppler waveforms. *Ultrasound Med Biol* 1988;14:365–76.
- [23] Hill AA, Surat DR, Cobbold RS, Langille BL, Mo LY, Adamson SL. A wave transmission model of the umbilicoplacental circulation based on hemodynamic measurements in sheep. *Am J Physiol* 1995;269:R1267–78.
- [24] Inan U, Inan A. *Engineering eElectromagnetics*. Upper saddle river, NJ: Prentice-Hall; 1998.
- [25] Avolio AP. Multi-branched model of the human arterial system. *Med Biol Eng Comput* 1980;18:709–18.
- [26] Gibson TC, Phernetton TM, Wiltbank MC, Magness RR. Development and use of an ovarian synchronization model to study the effects of endogenous estrogen and nitric oxide on uterine blood flow during ovarian cycles in sheep. *Biol Reprod* 2004;70:1886–94.
- [27] Park YW, Cho JS, Choi HM, Kim TY, Lee SH, Yu JK, et al. Clinical significance of early diastolic notch depth: uterine artery Doppler velocimetry in the third trimester. *Am J Obstet Gynecol* 2000;182:1204–9.
- [28] Milnor WR. *Hemodynamics*, 2nd ed., Baltimore: Williams & Wilkins; 1989.
- [29] Sprague BJ, et al. The effects of the ovarian cycle and pregnancy on uterine vascular impedance and uterine artery mechanics. *Eur J Obstet Gynecol* 2009;144:S170–8.
- [30] Nichols WW, O'Rourke MF. *McDonald's blood flow in arteries: theoretical, experimental, and clinical principles*, 5th ed., New York: Oxford University Press; 2005.
- [31] van den Wijngaard JP, Westerhof BE, Faber DJ, Ramsay MM, Westerhof N, van Gemert MJ. Abnormal arterial flows by a distributed model of the fetal circulation. *Am J Physiol Regul Integr Comp Physiol* 2006;291:R1222–33.
- [32] Guenther AE, Conley AJ, Van Orden DE, Farley DB, Ford SP. Structural and mechanical changes of uterine arteries during pregnancy in the pig. *J Anim Sci* 1988;66:3144–52.
- [33] Hees H, Moll W, Wrobel KH, Hees I. Pregnancy-induced structural changes and trophoblastic invasion in the segmental mesometrial arteries of the guinea pig (*Cavia porcellus* L.). *Placenta* 1987;8:609–26.
- [34] Magness R. Maternal cardiovascular and other physiologic responses to the endocrinology of pregnancy. In: Bazer, editor. *Endocrinology of pregnancy*. Humana Press; 1998.
- [35] Griendling KK, Fuller EO, Cox RH. Pregnancy-induced changes in sheep uterine and carotid arteries. *Am J Physiol* 1985;248:H658–65.
- [36] Osol G, Cipolla M. Interaction of myogenic and adrenergic mechanisms in isolated, pressurized uterine radial arteries from late-pregnant and nonpregnant rats. *Am J Obstet Gynecol* 1993;168:697–705.
- [37] Cipolla M, Osol G. Hypertrophic and hyperplastic effects of pregnancy on the rat uterine arterial wall. *Am J Obstet Gynecol* 1994;171:805–11.